Atmospheric Environment 62 (2012) 107–117

Contents lists available at SciVerse ScienceDirect

Atmospheric Environment

journal homepage: www.elsevier.com/locate/atmosenv

Detailed predictions of particle aspiration affected by respiratory inhalation and airflow

Kiao Inthavong [a], Qin Jiang Ge [a], Xiang Dong Li [a], Ji Yuan Tu [a,b,*]

[a] School of Aerospace, Mechanical and Manufacturing Engineering, RMIT University, Australia
[b] Department of Building Science, Tsinghua University, Beijing, China

HIGHLIGHTS

- Integrated model of human respiratory airway, humanoid, and indoor room is modelled.
- Flow near the face shows accelerated flow into the nostril during inhalation.
- Recirculating flow in the wake created behind body can induce pollutants.
- Particle tracking reveals origin of particles and its fate in respiratory airway.

ARTICLE INFO

Article history:
Received 13 June 2012
Received in revised form
23 July 2012
Accepted 30 July 2012

Keywords:
Air pollution
Particle
Deposition
Nasal cavity
Inhalation
CFD

ABSTRACT

The effects of air pollution found in the atmosphere and exposure to airborne particles are an important problem in the interest of public health. Exposure to contaminated air under different flow conditions is studied using the latest computational fluid dynamics models. For the first time the upper respiratory airway is integrated into a human body and placed inside a room, facing different airflow speeds (0.05 −0.35 m s^{-1}). It was found that the airflow streamlines diverged as it approached the human body, at the torso and accelerated upwards past the face and head before separating at the rear of the head, forming recirculating regions in the wake behind the body. Inhaled particles were tracked backwards to determine its origins. At a plane upstream from the face the locations of particles inhaled form a region known as the critical area, which is presented. This study establishes a better understanding of particle inhalability and provides a step towards a more holistic approach in determining inhalation toxicology effects of exposure to atmospheric particles.

1. Introduction

The study of the effects of air pollution found in the atmosphere and exposure to these airborne particles is an important problem in the interest of health effects associated with exposure to air pollution. Recently CFD (Computational Fluid Dynamics) simulations have been performed to investigate and visualise the flow patterns and local contaminant concentrations. These studies provide a deeper insight into particle dispersion given that many ventilation system designs are based on the assumption that airborne pollutants in the air are well-mixed within the room, which is not correct (Gadgil et al., 2003).

Studies have shown that localised concentrations and preferential flow regions are primarily caused by the room geometry (Lai et al., 2008; Zhang and Chen, 2006), and ventilation systems (Schlünssen et al., 2001). Particle dispersion studies in a room have been performed by Zhang and Chen (2009) using the Lagrangian particle tracking technique to determine exposure risk of building occupants to particulate matter. Other CFD studies have incorporated a human figure into the room (Poussou et al., 2010) which is a step towards a more integrated and realistic modelling approach to particulate exposure. Hayashi et al. (2002) placed a human occupant in a room to show the effects of contaminant inhalation, although the human face was simplified. It has been shown that inhaled particles from the external surroundings, referred to as the aspiration efficiency is influenced by facial features (Anthony et al., 2005). These studies recommend that CFD simulations should incorporate the complex features of the human face to adequately account for particle aspiration in low velocity environments.

* Corresponding author. School of Aerospace, Mechanical and Manufacturing Engineering, RMIT University, PO Box 71, Bundoora Vic 3083, Australia. Tel.: +61 3 9925 6191; fax: +61 3 9925 6108.
E-mail address: jiyuan.tu@rmit.edu.au (J.Y. Tu).

1352-2310/$ – see front matter © 2012 Elsevier Ltd. All rights reserved.
http://dx.doi.org/10.1016/j.atmosenv.2012.07.071

As the particles are inhaled, they are transported through the respiratory airways where some are deposited onto surrounding surfaces while some may navigate through the complex geometry and even reach the lung airways, causing deleterious health effects. Internal respiratory studies have been performed by the authors (Inthavong et al., 2009a, 2008, 2011c) among others (Liu et al., 2007; Schroeter et al., 2006) which has found that the transport and deposition of micron sized particles are dominated by its inertial property while submicron and nano sized particles are influenced by diffusion mechanisms. These studies are based on an isolated model of the human nasal cavity or tracheobronchial airway tree and as such the inlet boundary condition imposed at the nostril or trachea inlets are unknown and instead a blunt, parabolic or uniform profile is applied. Based on the aforementioned literature, it is apparent that there is a degree of independence and isolation amongst the cited studies which can be categorized into studies of: i) room and ventilation, ii) aspiration efficiency, iii) and particle deposition efficiencies in the respiratory airway. This leads to some loss in achieving a holistic set of results, which can greatly contribute towards new knowledge in identifying preventative measures for health risk exposure assessment.

Therefore this study presents an integrated CFD model simulation that combines the three aspects of contaminant exposure by including the external room, human occupant with realistic facial features, and the internal nasal–trachea airway. The influences of the external airflow patterns on the transport of indoor particle contaminants are evaluated. Visualisation of the air and particle flow patterns in the freestream and proximal to the nostrils are shown. By using a Lagrangian particle tracking technique, identification of the origins of the upstream particle locations that are inhaled (aspiration efficiency) are found. Furthermore the integrated model has the ability to correlate the contaminant source origin to the fate of the inhaled particle (i.e. particle deposition region in the respiratory airway).

2. Method

2.1. Computational geometry

A CT scan of the upper respiratory airway consisting of the nasal cavity, pharynx, larynx, and upper trachea from a 51 year old non-smoking Asian male provided the basis for reconstruction of a computational model. Segmentation of the desired airway was performed to extract a contiguous airway path from the nostril inlets to the upper trachea. Details of the segmentation method can be found in Inthavong et al. (2009b). In addition to the nostrils, a partial region of the external nose, proximal to the nostrils was included. A realistic human head was generated as an IGES file from FaceGEN Modeller (Singularity Inversion Inc., 2007) software, based on photographic images taken from a male volunteer. The three-dimensional (3D) head contained detailed facial features, such as shaped eyes, nose, mouth, and ears. Details of the facial features are given in Table 1 and are compared with the 50th percentile of a caucasian male as described in the literature (Huston, 2009; Zhuang et al., 2010). The comparisons show that the CFD model used in this study is slightly smaller than the 50th percentile for caucasian males.

The realistic head was placed onto a simple human body shape, and this was model placed into an empty room to simulate the ambient air. The three submodels (respiratory airway, human body, and surrounding room) were combined by importing the models into a CAD (Computer Aided Design) software modelling program and merged together. The final CAD model in Fig. 1 shows the upstream location (particle release plane) where a uniform concentration of particles is released from, detailed facial features, and the internal nasal-to-trachea respiratory airway cavity that is adjoined to the nostrils. A full human body model is used to include the torso which has been found to influence the particle aspiration (Anderson, 2010).

Table 1
Body and facial details.

Human occupant details			Facial details		
Dimension	Present study	50th% man[a]	Dimension	Present study	50th% man[b]
Occupant height	170.0	175.9	Head length	18.3	19.5
Mid shoulder height	139.7	144.4	Head circumference	56.3	56.8
Head width	13.5	15.5	Face length	9.1	11.8
Head depth	18.3	19.6	Face width	13.5	14.1
Top of head to chin	19.2	22.1	Nose length	4.13	5.0
Top of head to mouth centre	15.2	18.0	Nose protrusion	1.56	2.1
Top of head to eyes	9.2	11.5	Nose breadth	3.79	3.4

All units are in centimetres [cm].
[a] Huston (2009).
[b] Zhuang et al. (2010).

It is apparent that the model geometry spans over multiple length scales from metre lengths of the room down to centimetres within the airway bronchi. This presents a challenge in producing a quality computational mesh for CFD analysis. This step was also the most exhaustive stage in the CFD simulation process that involved meshing the model sequentially from the internal respiratory airway and outwards into the external room surrounding. Prism layers were applied to the bounding respiratory walls and a tetrahedral unstructured mesh filled the airway passage (Fig. 2a). The respiratory airway alone consisted of 11 million cells. In order to minimise the effects of numerical artificial diffusion (i.e. false diffusion) in the CFD simulation, the fine mesh resolving length scales in centimetres within the respiratory airway was gradually expanded out to length scales of metres to resolve the outer air in the room. Fig. 2b shows the different sections and aspects of the meshing as well as some cross-sectional outlines of the internal respiratory airways. The final number of cells in the mesh incorporating the respiratory airway, human body, and room was 16 million cells which used up 912 Mb in data storage size. Earlier studies by the authors have found that a mesh in excess of 2.0 million provided grid independence for the nasal cavity region (Inthavong et al., 2011a), while a mesh of 1.2 million was sufficient for grid independence for the room with human occupant model (King Se et al., 2010). Due to the large variation in length scales of the flow and geometry there is a greater demand on the computational mesh to minimise false diffusion caused by rapid changes in the mesh elements' size. To ensure quality of results, and a high level of mesh integrity, a mesh independence test was performed by investigating the velocity profiles at a number of different locations (e.g. inside the nasal cavity, in the near breathing region) until the profiles converged. The mesh became convergent at 8 million cells. However to minimise any false diffusion caused by the unstructured mesh a conservative the final computational model using 16 million cells was used. The visualisation and generation of the mesh was possible on a PC computer with 32 Gb Ram 2 Gb video card, and 8 processor cores. The simulations were performed on a High Performance Computing cluster which has 268 processor cores.

2.2. Airflow modelling

A steady oncoming freestream of air towards the human occupant was applied in order to investigate the '*worst case scenario*' for particle inhalability. This is confirmed by Kennedy and Hinds

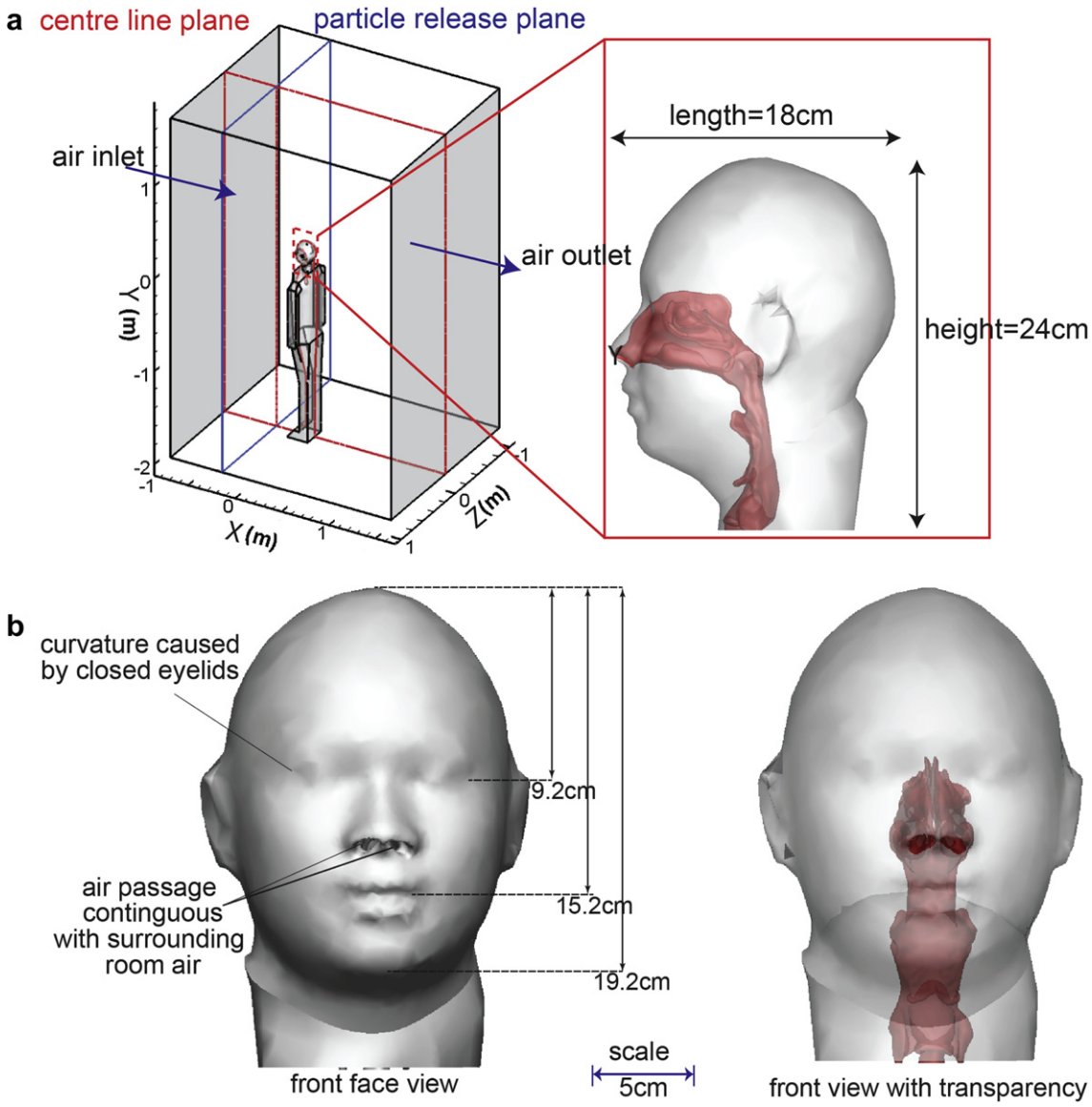

Fig. 1. (a) 3D CAD model incorporating the external surrounding room, human occupant, and the internal nasal–pharynx–larynx–trachea respiratory airway model. (b) Front view showing the detailed facial features. Geometry dimensions and details of the room and human occupant are given in Table 1.

(2002) which showed that the 'facing-the-wind' orientation produces an upper limit for inhalability compared with an averaged orientation which is produced by equally weighting particle inhalation over all angles from 0 to 360 orientation. The selection of the ambient airflow was based on the comprehensive survey of airflow speeds in indoor workplaces by Baldwin and Maynard (1998) which found a mean value of 0.3 m s^{-1} (ranging from 0.04 to 2.02 m s^{-1}) over all workplaces, however this value is skewed by measurements made in a wood drying shed that had a value of 1.79 m s^{-1}, and that neglecting this measurement produces a mean of 0.2 m s^{-1} (ranging from 0.04 to 0.72 m s^{-1}). More specifically for different workplace environments the mean values are: office 0.011–0.164 m s^{-1}; wood turning 0.064–0.119 m s^{-1}; heavy steel industry 0.063–1.737 m s^{-1}. Therefore in this study the influence of different indoor airflow velocities (0.05, 0.20 and 0.35 m s^{-1}) on the respiration and particle locations entering the nasal cavity via the nostrils. Table 2 provides a summary of the inhalation and room flow details.

Reynolds number matching over the head of the humanoid was applied in order to obtain dynamic similarity between the CFD simulation with existing experimental data in the literature by Anthony et al. (2005). For indoor airflows, reported results have shown much better flow separation and reattachment, which is an expected flow feature of the flow passing over the head, based on the k-ε-RNG model (Hofmann et al., 2003). But in the human

Table 2
Inhalation and room flow details.

Inhalation details			Room and ventilation details	
	Right	Left	Geometry	Dimension
Nostril openings	Area = 1.52 cm^2	Area = 1.31 cm^2	Length	250 cm
	Perim = 4.72 cm	Perim = 4.62 cm	Width	200 cm
	D_h = 1.288 cm	D_h = 1.134 cm	Height	350 cm

Dynamic similarity	Present study	Anthony et al. (2005)
$Re_{freestream}$ (room inlet)	48,000	50,250
Re_{head}	1850	1909
Head hydraulic diameter	14 cm	9.6 cm
$V_{freestream}$ (m s^{-1})	0.2 m s^{-1}	0.3

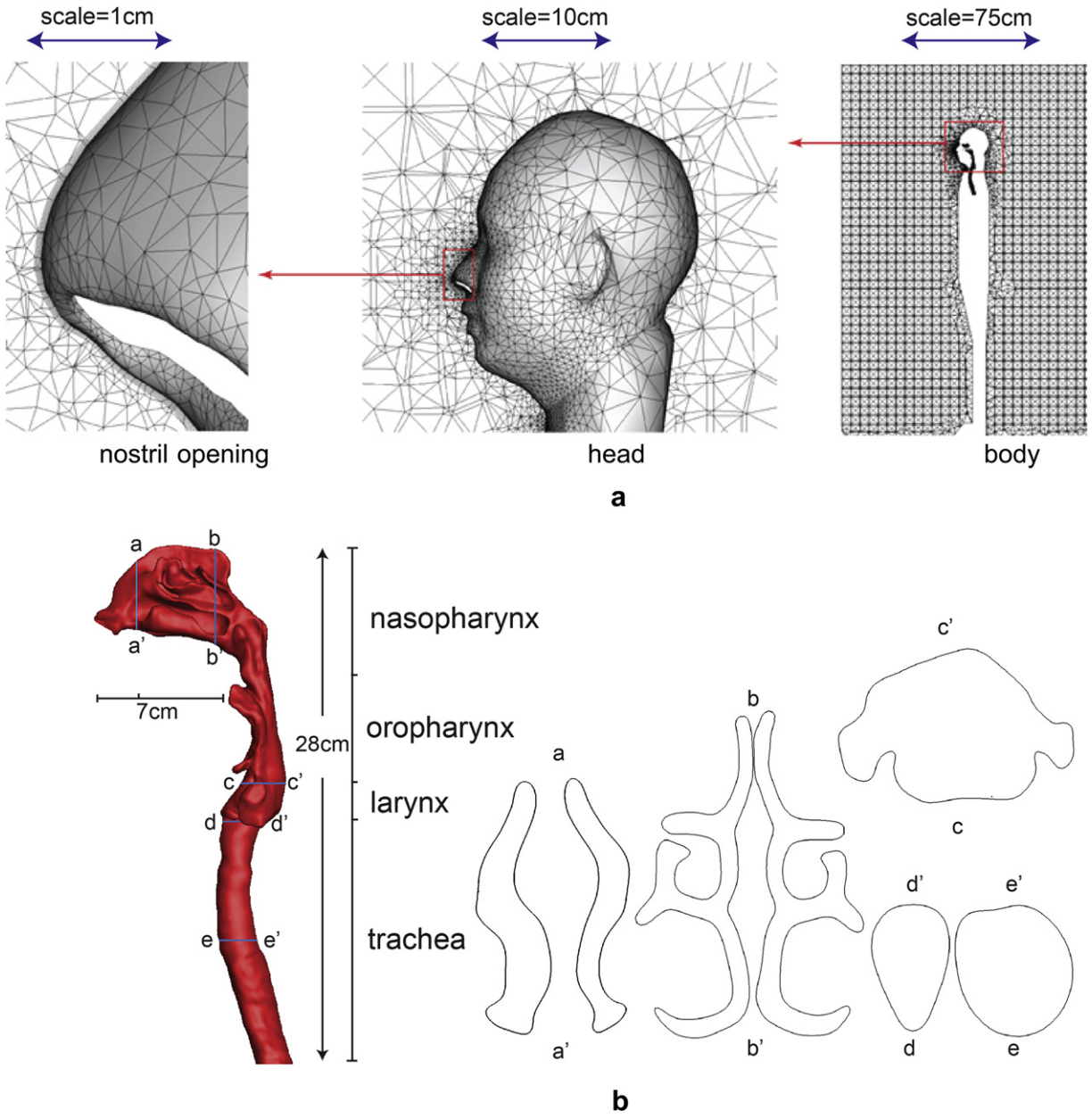

Fig. 2. (a) Mesh outline from close up view of the nostril opening, to the head, to the body inside the room. (b) Cross-sections labelled a–e taken at different locations within the internal upper respiratory airway which consists of the nasal cavity, pharynx, larynx, and trachea.

respiratory system, many researchers have used k-ω turbulent model with Shear Stress Transport (SST) developed by Menter et al. (2006) to analyse airflow in the nasal cavity (Wen et al., 2008; Zhang and Kleinstreuer, 2011). For respiratory inhalation, two flow rates of 15 and 40 L per minute (LPM) are presented for the aspiration efficiency through nasal inhalation, which represent light activity and heavy Airflow patterns in the respiratory airways, encounter a rich variety of flow structures existing in all three flow regimes of laminar, transition, and turbulent flow. Recently the four equation SST-transition model, along with an LES and laminar model were evaluated for its performance in predicting all three flow regimes in a constricted pipe and an idealized human oral airway model (Zhang and Kleinstreuer, 2011). The study found that there were no measurable differences between the turbulent models in predicting laminar flows as well as transition to turbulent flow. The SST-transition model is ideal for the internal respiratory flow; however its performance on the indoor airflow is unknown. This raises the issue of selecting a suitable turbulence model that will accommodate both the flow patterns in the indoor room air and inside the small respiratory airways. Given the successful implementation of the SST-transition model for respiratory airflows by Zhang and Kleinstreuer (2011), the model is first evaluated for indoor airflows against experimental data, a laminar model, and existing models that have proven successful such as the RNG k-ε, and LES. The continuity and momentum equations are given as:

Continuity equation:

$$\frac{\partial}{\partial x_i}\left(\rho_g u_i^g\right) = 0 \tag{1}$$

Momentum equation:

$$\rho_g u_i^g \frac{\partial u_i^g}{\partial x_j} = -\frac{\partial p_g}{\partial x_i} + \frac{\partial}{\partial x_j}\left[\mu_g \frac{\partial u_i^g}{\partial x_j}\right] \tag{2}$$

where, $\rho, \vec{U}$ and p are density, velocity, pressure of the air, respectively.

The turbulence model equations for the RNG k-ε model and the SST-transitional model are given in Isabey and Chang (1981) and Menter et al. (2006) from which the models are formulated, are not reproduced here for brevity. These equations are discretised using the finite volume CFD code, Fluent 13.0. The second order scheme is used to approximate the momentum equation whilst the pressure–velocity coupling is handled through the SIMPLE method.

2.3. Particle equations

Particles were released from a vertical plane 0.2 m upstream from the manikin face. Each individual particle is tracked from an upstream plane through the external space, and through the human respiratory system if they enter through the nostrils. A Lagrangian approach under one way coupling is used, and thus the particles are considered a dilute disperse phase. The particle tracking is terminated when the particles either reach a boundary surface, whereby the particle is assumed to deposit, or the particles escape through the computational domain via the trachea or the outlet boundary of the room. The force balance equation that governs the particle trajectory can be given as

$$\frac{du_p}{dt} = F_D(u_g - u_p) + \frac{g(\rho_p - \rho_g)}{\rho_p} \quad (3)$$

The drag force, F_D is dependent on the drag coefficient defined by

$$C_D = a_1 + \frac{a_2}{Re_p} + \frac{a_3}{Re_p^2} \quad (4)$$

where the *a's* are empirical constants for smooth spherical particles over several ranges of droplet Reynolds number (Morsi and Alexander, 1972). F_s represents other possible forces such as virtual mass force, Basset force, pressure gradient force, lift force, thermophoretic force and Brownian force. These forces are typically negligible for micron particles where $\rho_p >> \rho_g$. The number of particles tracked was checked for statistical independence since the turbulent dispersion is modelled based on a stochastic process. This was performed by sequentially increasing the number of particles so that the number that was inhaled increased to 50,000 particles. This was considered the optimum number for statistical independence since an increase of inhaled particles to 80,000 yielded a difference of 0.1% in the inhalation efficiency.

The turbulent dispersion on the particle is performed through the Discrete Random Walk (DRW) or "eddy interaction model". This approach assumes that a particle interacts with a succession of random discrete turbulent eddies, where each eddy is defined by a lifetime, length, and velocity scale. The velocity scale is determined by a Gaussian distributed random velocity of the turbulent kinetic energy, k given by:

$$u'_e = \zeta(2k/3)^{0.5} \quad (5)$$

where ζ is a random Gaussian random number with mean zero and unit variance. The k-ε and k-ω family of turbulent models are classified as Reynolds-Averaged-Navier–Stokes (RANS) based models that assume the turbulent fluctuations are isotropic in all directions (i, j, k). In the turbulent core region, this isotropic assumption is valid in the absence of high swirls and rapid changes in the strain rate; however close to the wall, the turbulent flow character is highly anisotropic. An improved model for the random walk method is to apply a damping function to correct the fluctuations in the near wall up to y^+ of 60 as

$$k_{new} = \left[1 - \exp\left(-0.02y^+\right)\right]^2 k \quad \text{for } y^+ < 60 \quad (6)$$

Full details of the scheme can be found in Inthavong et al. (2011a) and Inthavong et al. (2011b) which implemented the damping function to improve the micron particle deposition in the nasal cavity (Fig. 3).

3. Results and discussion

3.1. Velocity vectors in the breathing region

Velocity vectors in the x–y plane passing through at $z = 0$ cm through the middle of the nose (Fig. 4a) are compared with reported experimental data by Anthony et al. (2005) and computational data from King Se et al. (2010). The ambient flow rate is set to 0.3 m s^{-1} to match the comparative data. The resultant flow field reported by Anthony et al. (2005) using Particle Image Velocimetry (PIV) data in the near breathing region showed vectors pointing vertically upwards, caused by the presence of the torso where the airstream diverges as it flows past the body. As the inhaled air approaches the face, the vectors converge towards the mouth by the inhalation, or passes over the nose and the upper regions of the face. The CFD simulation shows good qualitative comparisons with the reported data. Close to the mouth, the oncoming airflow bifurcates at the nose tip as well as at the chin. Downwards flow is found in the philtrum (space between the nose and the upper lip). The significance of using realistic facial features is that the region close to the mouth show the vectors that are directed towards the mouth from the philtrum (just above the upper lip) occurs earlier in the horizontal plane for the realistic facial feature model (confirmed with the present study) in comparison with a cylindrical human form (Anthony et al., 2005).

The corresponding normalized velocity profiles taken at $x = 1$ cm and $x = 1.5$ cm upstream from the face are shown in Fig. 4b. The figure also includes additional results obtained from the human body in a room but for a shorter upstream distance (F:20 cm R:150 cm) and also a shorter downstream distance (F:100 cm R:50 cm). The letters F represents frontal distance from nose tip, and R, the rear distance from the nose tip. This is performed to ensure that the most optimal geometry is used (i.e. computational efficiency), since it is uncertain if a smaller volume surrounding the face is sufficient or if there is a need to model the upper respiratory system within an entire full room. The base model is F:100 cm R:150 cm, and its profile under both the SST transitional and RNG turbulence models are similar. Some differences in the profiles are found when using either a shorter upstream or downstream length which suggests that a full room model is needed.

Comparisons with the data in the literature show good agreement between the profiles, especially at $x = 1.5$ cm. The location of the mouth is located at the normalized vertical distance of 0.5, which also corresponds to the maximum velocity where the flow has accelerated from the chin and upper lip regions. Minimum velocities near the stagnation point at the nose tip height is found at the normalized vertical distance of $y = 0.8$ for both planes. Slight differences are found in the chin region below the lower lip and also in the philtrum, which may be attributed to some differences in the exact facial features.

For nasal inhalation, airflow is now directed upwards towards the nostril openings (Fig. 4). The velocity vectors show that the inhaled flow is nearly all directed vertically into the nostrils. This suggests that low inertia particles will drift with the induced airflow. Particles with higher inertia and mass, that aren't able to drift with the flow streams, need to be found above the nostrils allowing gravitational settling to occur in order to for the particles

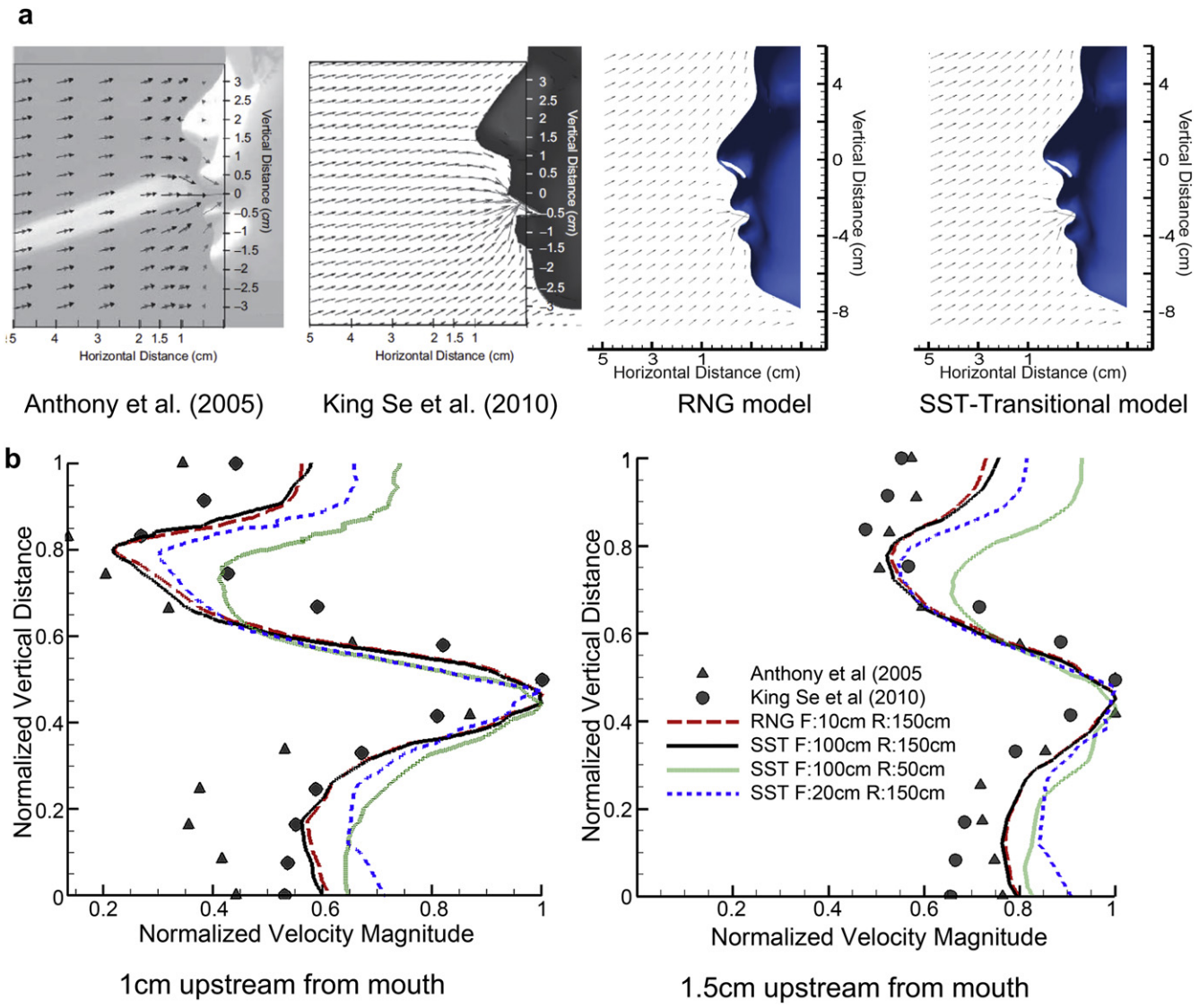

Fig. 3. Velocity vector plots for oral inhalation using (a) CFD and PIV experimental measurements from Anthony et al. (2005). (b) Velocity magnitude profiles at upstream locations of 1 cm and 1 cm from the nose tip.

to be inhaled into the respiratory system. The effect of the vertical flow across the closed mouth region can enhance the inhalability of the particles if breathing through the mouth was also to occur midway through an inhalation cycle. Such a study involving both the nose and mouth inhalation under different breathing situations was not investigated in this paper and is left for future studies.

The velocity profiles in Fig. 4b show a shift in the stagnation regions where the flow bifurcates near the chin is higher for nasal inhalation in comparison with oral inhalation. The comparisons of velocity profiles with data from King Se et al. (2010) show good agreement. In both oral and nasal inhalation, sharp acceleration of the inhaled air occurs as it approaches the mouth or nose, which will contribute additional momentum to inhaled particles, thus greatly enhancing the likelihood of early particle deposition (Fig. 5).

3.2. *Influence of ambient flow rate*

Particle aspiration efficiencies have been defined as the fraction of particles that are inhaled through the nose or mouth during breathing (Vincent et al., 1990), which is also referred to as 'inhalability'. Factors that influence particle aspiration efficiency include the particle size and the external ambient airflow around the human body. In the cases presented in this study, the human body is facing the oncoming air which transports the particles from upstream towards the breathing region. Fig. 6 shows the oncoming air diverging at the torso as it approaches the body, thus the air that is inhaled comes from underneath the face, rather than above. This implies that airborne particles that are present below the breathing region are more likely to be inhaled. Furthermore the inhalation streamlines show that for a lower ambient airflow rate, a larger region of air (i.e. air '*stream-tube*') is inhaled, in comparison to a higher ambient airflow rate. Under both conditions the inhaled air is being pulled from below the breathing region.

The airflow accelerates around the head of the body, the boundary layer separates at the rear, producing a wake, with a recirculation region forming just behind the head. An increase in the ambient airflow rate produces a recirculation region that is further from the body. This study only investigated the inhalability of particles from an upstream source of airflow, however the results of the wake flow shown in Fig. 6 indicate that if the ambient airflow was coming from behind the body, particles from a contaminant source in front of the body may be disturbed and induced into the

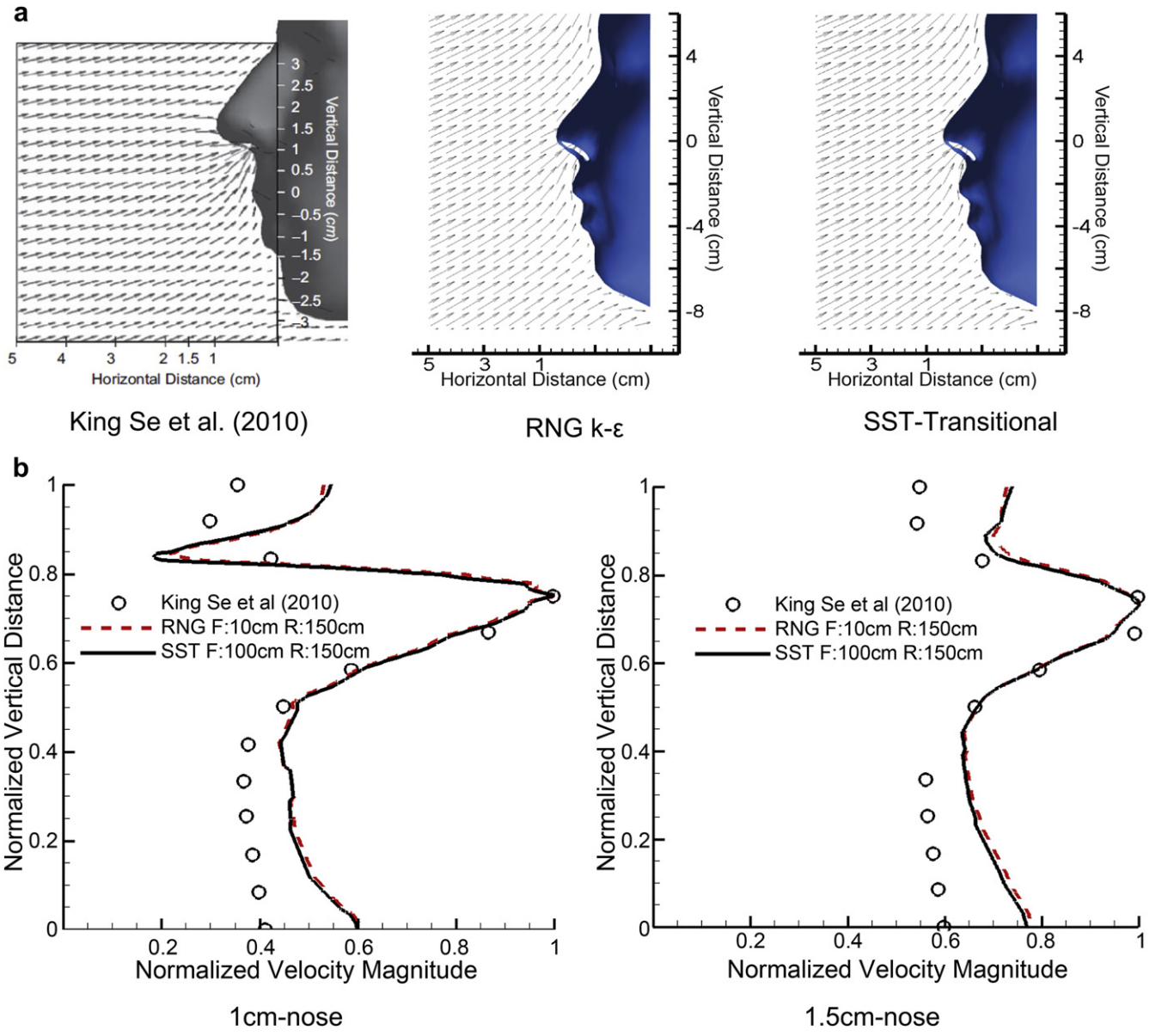

Fig. 4. Velocity vector plots for (a) CFD oral inhalation and (b) PIV experimental measurements from Anthony et al. (2005). (c) CFD nasal inhalation. Ambient surrounding flow rate is 0.2 m s^{-1}.

breathing region, and thus enhancing the inhalability of the particles. The wake region can induce a well-mixed scenario through the presence of vortices that can entrain air.

3.3. Particle inhalation trajectory

Particle trajectories originating from a plane located at a distance of 0.2 m upstream from the nose tip are shown in Fig. 6 for ambient airflow rates of 0.05 m s^{-1} and 0.35 m s^{-1}. The results for the airflow rate of 0.2 m s^{-1} are not shown as they lie in between the results for airflow rates of 0.05 m s^{-1} and 0.35 m s^{-1} as expected. The vertical distance coordinate is set to $y = 0$ m at the nostril level, so that the trajectories of nasal inhaled particles converge to this point. The trajectories show that for 40 μm and 80 μm sized particles, gravitational settling dominates where the particle source originates from a much higher vertical position in relation to the nostril openings. The trajectory of these particles is linear until they reach the nose where acceleration towards the nostril occurs due to nasal inhalation. This linearity means that the location of the particle source for large particles may be identified for a given upstream distance through extrapolation. The further upstream the distance, the higher the vertical distance should be for the particles to descend towards the nose.

At higher ambient airflow rates the vertical distance needed for 40 μm and 80 μm particles to overcome gravitational settling is reduced significantly from 0.65 m down to 0.05 m due to the horizontal momentum component induced by the airflow. Smaller particles such as 1–20 μm all possess much lighter masses and therefore its low inertia allows the particles to be influenced by the surrounding flow field. This leads to particles tending to follow the airflow streamlines more and the upstream location of the particle source is now located at a vertical distance of 0.05–0.1 m below the nostrils, since it was shown earlier that the flow streamlines diverge at the torso region as the flow approaches the human body. At the higher ambient airflow rate the trajectories of the smaller particles do not change significantly.

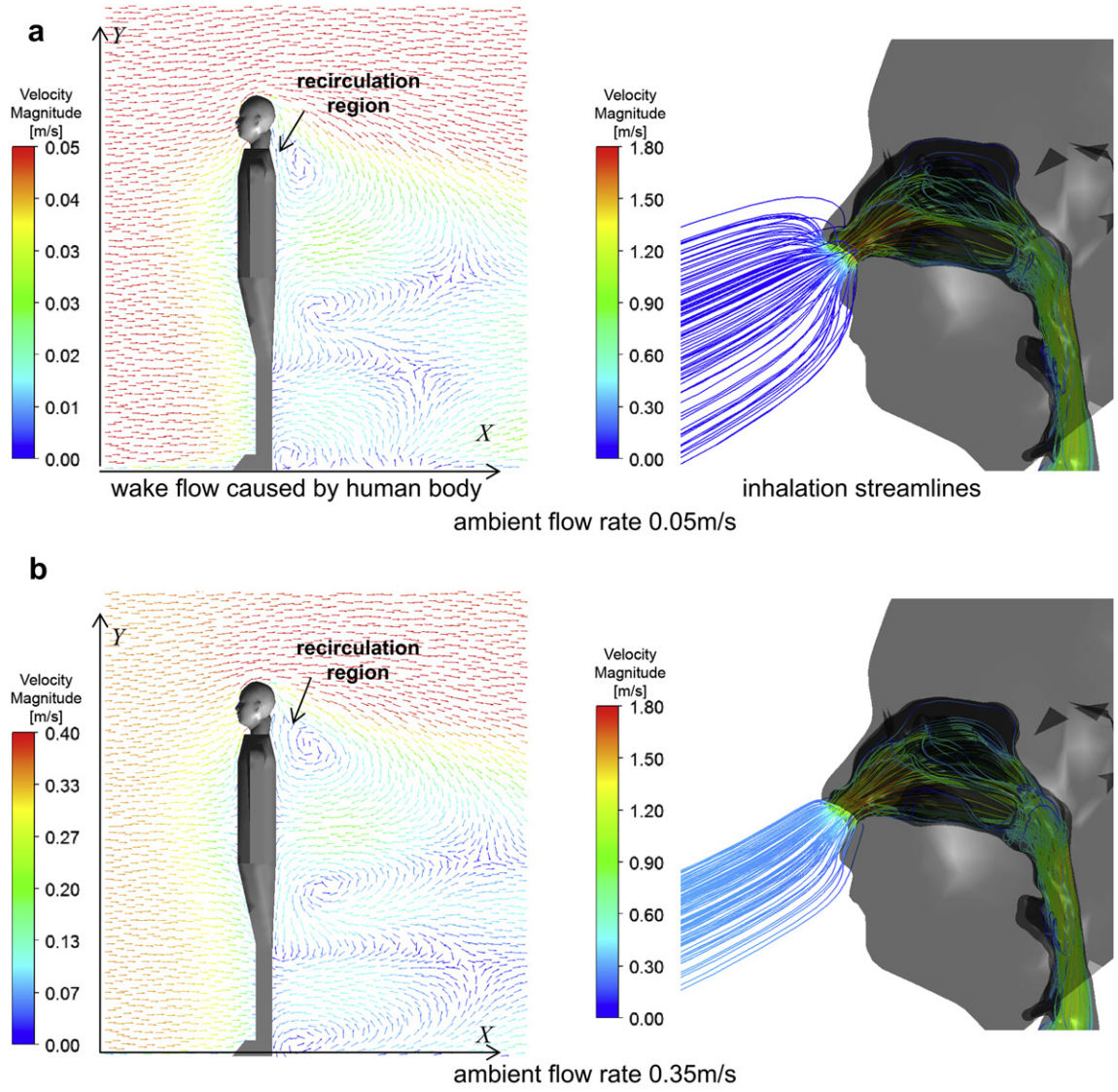

Fig. 5. Velocity vectors in the centreline plane showing the flow field around the humanoid (left). Streamtubes showing the region of air that is inhaled through the nostrils and into the respiratory system (right). The inhalation rate of the nostrils at 15 L min^{-1}.

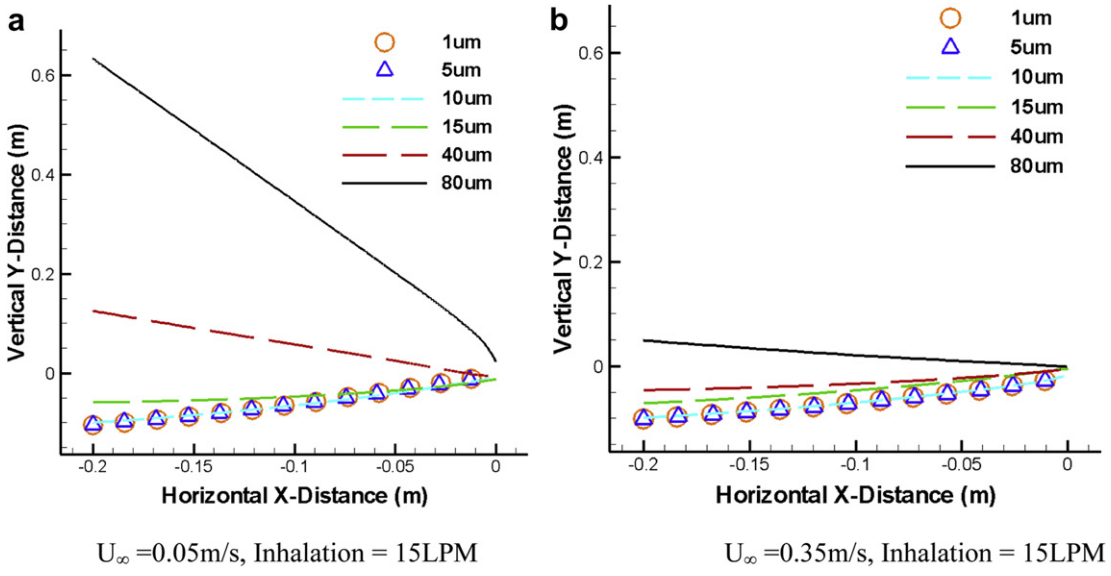

Fig. 6. Sample trajectory of inhaled particles released at 0.2 m upstream for different particle sizes and ambient.

3.4. Particle deposition patterns

The critical area is defined as the region with which particles are inhaled from at a given location upstream from the human body (Anthony et al., 2005). At the upstream location of 0.2 m from the nostril inlets, the critical areas representing the source of inhaled particles show two distinct regions which is caused by the two different nostrils inlets (Fig. 7). The critical areas are viewed from

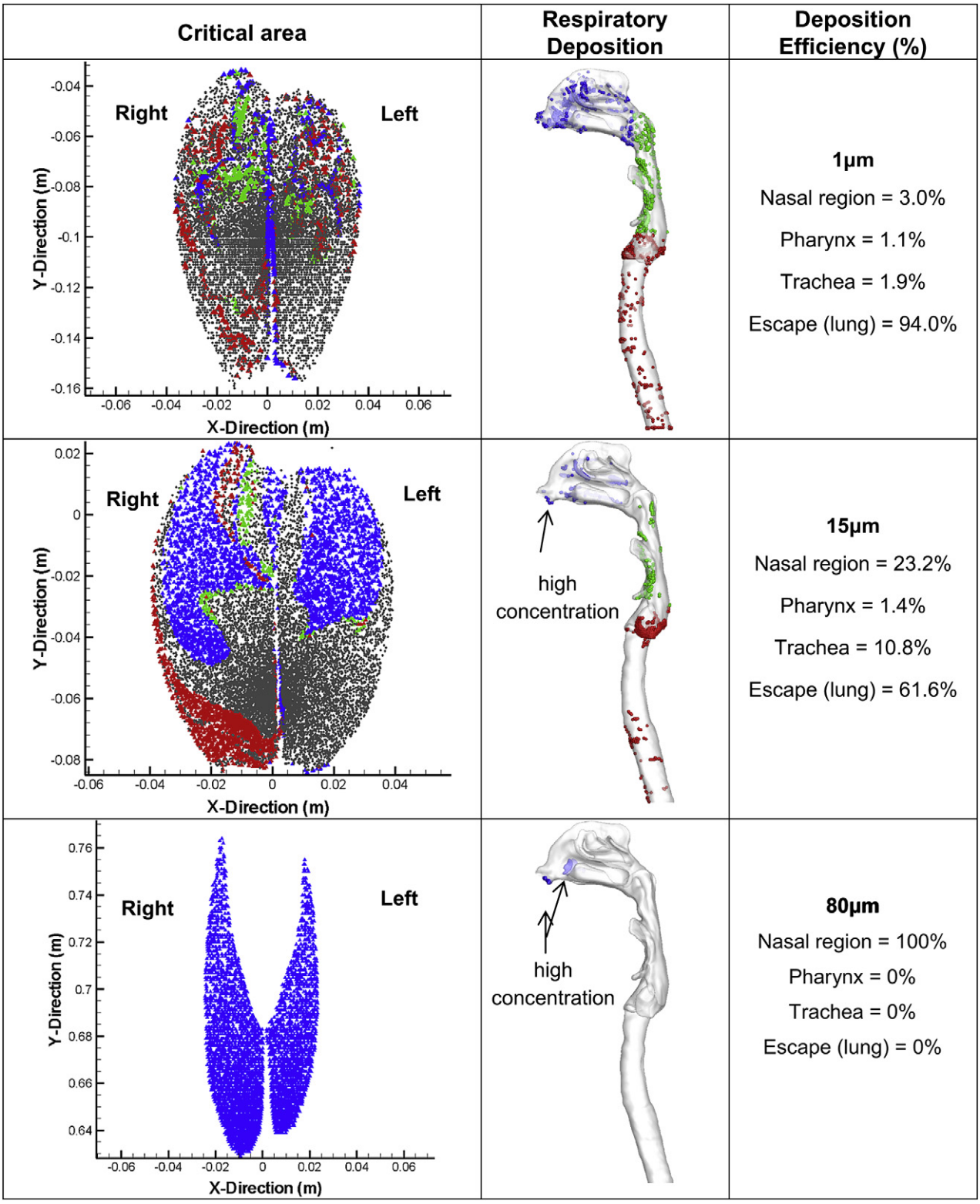

Fig. 7. Critical areas for the upstream particle release plane at $x = 0.20$ m (see 'Particle Release Plane' in Fig. 1) for inhaled particles and its deposition in the upper respiratory airway for ambient airflow rate of 0.05 m s^{-1}.

upstream and the labelling convention is to name the left and right critical areas consistent with the same side they sit anatomically with the human body involved. Thus the left critical area is mainly influenced by the left nostril and left nasal chamber that produces the inhalation effort.

Each individual particle that is inhaled through the nostril is tracked via the Lagrangian tracking equation (Eqn. (3)) and the particle deposition onto the respiratory surface is recorded. The accuracy of the particle tracking algorithm was evaluated based on the particle deposition efficiency against the inertial parameter (IP), defined as $IP = Q \times d^2$, where Q is the inhalation flow rate ($cm^3\ s^{-1}$), and d is the aerodynamic particle diameter (μm). It was found that using the damping function to correct the turbulent fluctuations in the near wall (Equation (6)) provided sufficiently accurate results which can be found in Inthavong et al. (2011a, 2011b).

The blue coloured particles represent those particles depositing onto the nasal cavity region; the green particles deposit onto the pharyngeal region; the red particles deposit onto the trachea; and the grey particles are those that don't deposit and in fact escape from the respiratory geometry and enter the bronchial regions of the lungs. For 1 μm particles, there is no distinguishable pattern from the critical area that can allow confident predictions of where a particle may deposit within the respiratory airway.

For 15 μm particles nearly all the particles that deposit in the trachea region originate from the left side of the critical area. This suggests that particles that enter the left nasal chamber, and take on that particular pathway will experience and be influenced by a different airflow pattern if the particles had entered the right-hand nasal chamber. During normal nasal physiology, the nasal cavity is asymmetrical where one nasal passage is typically more patent than the other. This asymmetry is referred to as the nasal cycle which is a result of congestion (swelling) of the erectile tissue (cavernous tissues of the mucosa) in one nasal cavity while at the same time decongestion (shrinking) occurs to the erectile tissue in the other cavity. The airflow through each nasal cavity is then governed by the resistance caused by the cross-sectional area of each airway. This asymmetry may explain the bias for those particles that exist in the lower left region of the critical area to deposit in the trachea region.

A second pattern that emerges from the 15 μm critical area is that the blue coloured particles (depositing in the nasal cavity region) exist in the upper half of the critical area, compared with the red coloured particles (depositing in the trachea) which exist in the lower half of the critical area. It has been established that for 15 μm sized particles early deposition in the nasal cavity is attributed to inertial deposition (Inthavong et al., 2006; Wang et al., 2009), where particles that exhibit high momentum will not follow the airflow streamlines. In Fig. 6 it was shown that as the particles accelerated as they approached the nostrils, due to the inhaled air that complements the oncoming airflow. In addition particles originating from above the nostrils are further accelerated by the gravitational pull which becomes more influential as the particles become larger in size. These two contributing factors cause the particles to exhibit higher inertia as they enter the respiratory domain, when compared to those particles that originate from below the nostrils. A further investigation found that a large number of those particles that deposited in the nasal region (total = 23.2%) are concentrated at or near the nostril inlet, and is labelled in Fig. 7 with arrows pointing to these high concentration regions.

For 80 μm particles the larger mass of the particle means that it is highly influenced by gravitational settling, and therefore the critical areas at the upstream location are located at a much higher vertical distance from the nostril inlets. Similar to the 15 μm particles, the 80 μm particles are further accelerated due to the inhaled air that complements the oncoming airflow, thereby increasing its inertial properties even further. This creates regions of high concentration of particles depositing at or near the nostril inlets (arrows pointing to high concentration region). The shape of the critical area is that of two narrow teardrops where a larger concentration of particles is found near the bottom of the critical area.

4. Conclusion

An integrated CFD model simulation was performed to better understand the air and particle flow patterns in human exposure to indoor air pollutants. A realistic upper respiratory airway model based on CT-scans was created and integrated into a human body. During inhalation, the flow patterns near the face show vertically aligned flow streams which transport the particles towards either the nose during nasal inhalation or mouth during oral inhalation. An influence of the ambient airflow rate on the flow patterns is the increased acceleration of flow that begins as the airflow diverges at the torso. Flow separation occurs at the rear of the human head and there is a shift in the recirculation region, and different wake effects are found. This indicates that if the ambient airflow was coming from behind the body, particles form a contaminant source in front of the body may be disturbed and induced into the breathing region. Trajectories of the inhaled particles found that the source of large inhaled particles (e.g. 40 μm and 80 μm) that are originating from upstream must be above the nose as gravitational settling is significant for these particles. For the smaller particles (1–20 μm), particles tend to follow the flow streamlines and their original upstream location must be below the nostrils. The critical area shapes were determined by reverse tracking the particles to its origins and colour coding their positions in order to determine if a pattern could be deduced for predictions of local respiratory region deposition. It was found that only the 15 μm particle size produced discernible pattern. This study aimed to establish a better understanding of particle inhalability and to enhance the state of the art CFD modelling towards a holistic simulation for exposure of airborne particles.

Acknowledgements

The authors gratefully acknowledge the financial support provided by the National Basic Research Program (973) of China, Grant No. 2012CB720100 and the Australian Research Council (project ID: DP120103958).

References

Anderson, K.R., 2010. Computational Fluid Dynamics (CFD) Study Investigating the Effects of Torso Geometry Simplification on Aspiration Efficiency. Department of Occupational and Environmental Health, The University of Iowa, Iowa.

Anthony, T.R., Flynn, M.R., Eisner, A., 2005. Evaluation of facial features on particle inhalation. Annals of Occupational Hygiene 49, 179–193.

Baldwin, P.E.J., Maynard, A.D., 1998. A survey of wind speeds in indoor workplaces. Annals of Occupational Hygiene 42, 303–313.

Gadgil, A.J., Lobscheid, C., Abadie, M.O., Finlayson, E.U., 2003. Indoor pollutant mixing time in an isothermal closed room: an investigation using CFD. Atmospheric Environment 37, 5577–5586.

Hayashi, T., Ishizu, Y., Kato, S., Murakami, S., 2002. CFD analysis on characteristics of contaminated indoor air ventilation and its application in the evaluation of the effects of contaminant inhalation by a human occupant. Building and Environment 37, 219–230.

Hofmann, W., Golser, R., Balashazy, I., 2003. Inspiratory deposition efficiency of ultrafine particles in a human airway bifurcation model. Aerosol Science and Technology 37, 988–994.

Huston, R.L., 2009. Principles of Biomechanics. CRC Press. 9780849334948.

Inthavong, K., Tian, Z.F., Li, H.F., Tu, J.Y., Yang, W., Xue, C.L., Li, C.G., 2006. A numerical study of spray particle deposition in a human nasal cavity. Aerosol Science and Technology 40, 1034–1045.

Inthavong, K., Wen, J., Tian, Z., Tu, J., 2008. Numerical study of fibre deposition in a human nasal cavity. Journal of Aerosol Science 39, 253–265.

Inthavong, K., Tu, J.Y., Ahmadi, G., 2009a. Computational modelling of gas-particle flows with different particle morphology in the human nasal cavity. Journal of Computational Multiphase Flows 1, 57–82.

Inthavong, K., Wen, J., Tu, J.Y., Tian, Z.F., 2009b. From CT scans to CFD modelling – fluid and heat transfer in a realistic human nasal cavity. Engineering Applications of Computational Fluid Mechanics 3, 321–335.

Inthavong, K., Ge, Q., Se, C.M.K., Yang, W., Tu, J.Y., 2011a. Simulation of sprayed particle deposition in a human nasal cavity including a nasal spray device. Journal of Aerosol Science 42, 100–113.

Inthavong, K., Tu, J., Heschl, C., 2011b. Micron particle deposition in the nasal cavity using the v2–f model. Computers & Fluids 51, 184–188.

Inthavong, K., Zhang, K., Tu, J., 2011c. Numerical modelling of nanoparticle deposition in the nasal cavity and the tracheobronchial airway. Computer Methods in Biomechanics and Biomedical Engineering 14, 633–643.

Isabey, D., Chang, H.K., 1981. Steady and unsteady pressure-flow relationships in central airways. Journal of Applied Physiology 51, 1338–1348.

Kennedy, N.J., Hinds, W.C., 2002. Inhalability of large solid particles. Journal of Aerosol Science 33, 237–255.

King Se, C.M., Inthavong, K., Tu, J., 2010. Inhalability of micron particles through the nose and mouth. Inhalation Toxicology 22, 287–300.

Lai, A.C.K., Wang, K., Chen, F.Z., 2008. Experimental and numerical study on particle distribution in a two-zone chamber. Atmospheric Environment 42, 1717–1726.

Liu, Y., Matida, E.A., Junjie, G.U., Johnson, M.R., 2007. Numerical simulation of aerosol deposition in a 3-D human nasal cavity using RANS, RANS/EIM, and LES. Journal of Aerosol Science 38, 683–700.

Menter, F.R., Langtry, R.B., Likki, S.R., Suzen, Y.B., Huang, P.G., Volker, S., 2006. A correlation-based transition model using local variables – part I: model formulation. Journal of Turbomachinery 128, 413–422.

Morsi, S.A., Alexander, A.J., 1972. An investigation of particle trajectories in two-phase flow systems. Journal Fluid Mechanics 55, 193–208.

Poussou, S.B., Mazumdar, S., Plesniak, M.W., Sojka, P.E., Chen, Q., 2010. Flow and contaminant transport in an airliner cabin induced by a moving body: model experiments and CFD prediction. Atmospheric Environment 44, 2830–2839.

Schlünssen, V., Vinzents, P.S., Mikkelsen, A.B., Schaumburg, I., 2001. Wood dust exposure in the Danish furniture industry using conventional and passive monitors. Annals of Occupational Hygiene 45, 157–164.

Schroeter, J.D., Kimbell, J.S., Asgharian, B., 2006. Analysis of particle deposition in the turbinate and olfactory regions using a human nasal computational fluid dynamics model. Journal of Aerosol Medicine 19, 301–313.

Vincent, J.H., Mark, D., Miller, B.G., Armbruster, L., Ogden, T.L., 1990. Aerosol inhalability at higher windspeeds. Journal of Aerosol Science 21, 577–586.

Wang, S.M., Inthavong, K., Wen, J., Tu, J.Y., Xue, C.L., 2009. Comparison of micron- and nanoparticle deposition patterns in a realistic human nasal cavity. Respiratory Physiology and Neurobiology 166, 142–151.

Wen, J., Inthavong, K., Tu, J.Y., Wang, S., 2008. Numerical simulations for detailed airflow dynamics in a human nasal cavity. Respiratory Physiology & Neurobiology 161, 125–135.

Zhang, Z., Chen, Q., 2006. Experimental measurements and numerical simulations of particle transport and distribution in ventilated rooms. Atmospheric Environment 40, 3396–3408.

Zhang, Z., Chen, Q., 2009. Prediction of particle deposition onto indoor surfaces by CFD with a modified Lagrangian method. Atmospheric Environment 43, 319–328.

Zhang, Z., Kleinstreuer, C., 2011. Laminar-to-turbulent fluid-nanoparticle dynamics simulations: model comparisons and nanoparticle-deposition applications. International Journal for Numerical Methods in Biomedical Engineering 27, 1930–1950.

Zhuang, Z., Landsittel, D., Benson, S., Roberge, R., Shaffer, R., 2010. Facial anthropometric differences among gender, ethnicity, and age groups. Annals of Occupational Hygiene 54, 391–402.